A unified view of imaging the elastic properties of tissue

Kevin J. Parker, Lawrence S. Taylor, and Sheryl Gracewski
School of Engineering and Applied Sciences, University of Rochester, P.O. Box 270126, Rochester, New York 14627-0127

Deborah J. Rubens
Department of Radiology, University of Rochester Medical Center, 601 Elmwood Avenue, Rochester, New York 14642-8648

~Received 8 April 2004; revised 24 January 2005; accepted 28 January 2005!

A number of different approaches have been developed to estimate and image the elastic properties of tissue. The biomechanical properties of tissues are vitally linked to function and pathology, but cannot be directly assessed by conventional ultrasound, MRI, CT, or nuclear imaging. Research developments have introduced new approaches, using either MRI or ultrasound to image the tissue response to some stimulus. A wide range of stimuli has been evaluated, including heat, water jets, vibration shear waves, compression, and quasistatic compression, using single or multiple steps or low-frequency ~<10 Hz! cyclic excitation. These may seem to be greatly dissimilar, and appear to produce distinctly different types of information and images. However, our purpose in this tutorial is to review the major classes of excitation stimuli, and then to demonstrate that they produce responses that fall within a common spectrum of elastic behavior. Within this spectrum, the major classes of excitation include step compression, cyclic quasistatic compression, harmonic shear wave excitation, and transient shear wave excitation. The information they reveal about the unknown elastic distribution within an imaging region of interest are shown to be fundamentally related because the tissue responses are governed by the same equation. Examples use simple geometry to emphasize the common nature of the approaches.
@DOI: 10.1121/1.1880772#

PACS numbers: 43.80.Qf, 43.80.Ev, 43.80.Jz @FD# Pages: 2705–2712

I. INTRODUCTION

The biomechanical properties of tissues, particularly the stiffness or tactile hardness of tissues, are inextricably linked to the function, the composition, and the mentarEC58c04.8he

material. It is shown that the elastic response within the material under the different stimuli all belong within a common spectrum of elastic behavior, and some information concerning the inclusion can be derived from each of the responses to the stimuli.

wave speed $c_s = \sqrt{E/3\rho}$ can be used to obtain information about the stiffness of the material. Therefore, in elastographic imaging experiments, the focus of attention is typically on the shear wave properties and not on pressure wave properties, which have already been investigated extensively in ultrasonic tissue characterization studies.

Equation (6) can also be a starting point for the consideration of step-compression elastography experiments. For static displacement or very low-frequency cyclic motion, the inertial terms are negligibly small. And for nearly incompressible biomaterials, the divergence (or dilatation) $\nabla\cdot\mathbf{u}$ is nearly zero, so Eq. (6) reduces to Laplace's equation,

$$\nabla^2\mathbf{u}=\mathbf{0}. \tag{11}$$

Solutions to Laplace's equation depend on and reach their extrema on the boundary values of $\mathbf{u}$. For simple geometry, as will be shown in the next section, the solution for $u_x(x)$ is linear with x, a fact that is assumed to be true in most step-compression elastographic imaging experiments.

III. PROPOSED TECHNIQUES FOR ESTIMATING ELASTIC PROPERTIES OF TISSUES

A. Step-compression imaging

For convenience we consider a two-dimensional case of a linear viscoelastic, homogeneous, isotropic material with tissue mimicking properties: E_0 in the kPa range, ρ (density) near 1.0 g/cm^3, and ν (Poisson's ratio) in the range $0.49<\nu<0.5$, that is, nearly incompressible. This block of tissue-mimicking material is of a rectangular cross section and is rigidly constrained along one face and further constrained by a parallel plate used for compression or other enforced displacements. We further assume that the tissue mimicking material is allowed to slip freely along the two constraining plates so that the displacement and stress fields will be independent of position in the y direction. Body forces due to gravity are assumed to be negligible. The example is shown in Fig. 1.

We assume that compression is applied at time t_0, and that images are obtained using some ideal imaging system, before and after the compression step. In the case of viscoelastic or poroelastic materials, the state of the material response and its image will be time dependent until sufficient relaxation has occurred. Assuming that a dense field of displacements can be estimated from the two images, in the homogeneous case, Eq. (11) predicts that the displacement $u_x(x)$ will be linear with x, as shown in Fig. 1(b) (solid lines). In the case where a small inhomogeneous region of $E'>E_0$ (assumed here to be of relatively small contrast $E'/E_0<2$), is present, a plot of displacement taken on a line bisecting the inhomogeneity will produce a local deviation from the linear slope. The exact details depend on the precise geometry and the stress concentration effect,[34] but the general trend is shown in Fig. 1(b) (dotted lines).

(b)

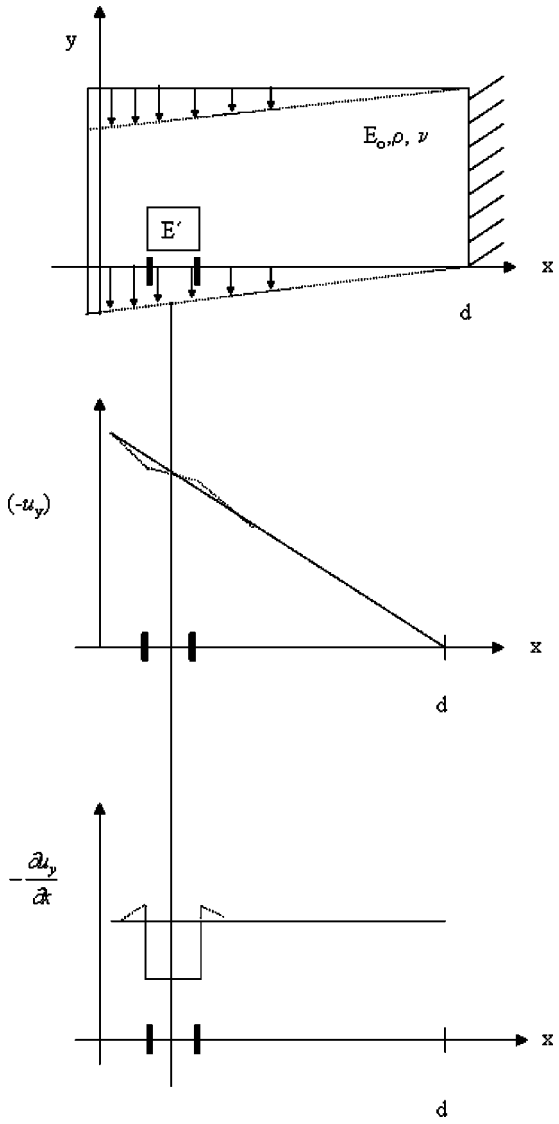

FIG. 2. Static shear experiment on a same block shown in Fig. 1: ~a! Block before ~solid lines! and after ~dotted lines! shear by a rigid plate. ~b! Shear displacement field ~u_y; vertical axis! along a line parallel to the x-axis through the small rectangular inclusion. ~c!

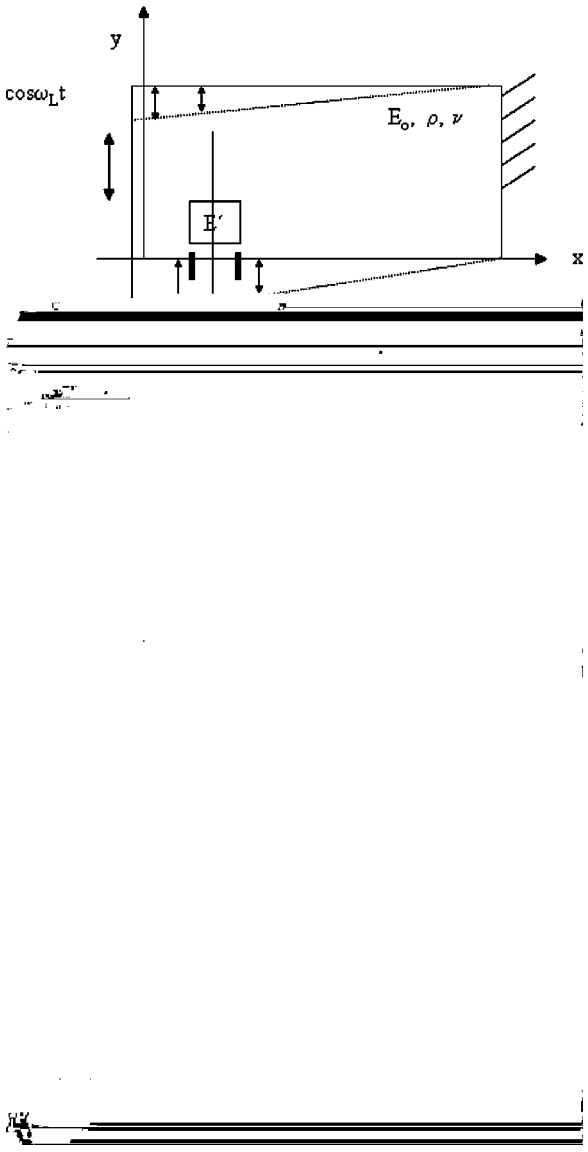

FIG. 3. Cyclical quasi-static shear experiment on the block shown of Fig. 1: ~a! Block before ~solid lines! and at peak ~dotted lines! shear. The applied shear is sinusoidal at low frequency. ~b! Peak shear displacements ~solid line!, along a parallel to the x-axis through the small rectangular inclusion, are linear but slowly time-varying. ~c! Peak shear strain along this line is also slowly time-varying. The dotted lines indicate the perturbation caused by the presence of inhomogeneity.

complementary to the compression result when one considers the uniqueness of inverse solutions from these experiments. However, the details of that subject are beyond the scope of this discussion. As in the compression step results, Eq. ~11! predicts that for a homogeneous medium displacement, $u_y(x)$ will be linear with x, which can be perturbed by an inclusion. As before, the exact details of the shear in the vicinity of the inclusion require treatment of the exact geometry and elastic contrast of the inclusion. However, stress concentration effects are highly localized in the surrounding medium. As demonstrated in Fig. 2, a spatial derivative can be employed to produce a more intuitive display where homogeneous regions exhibit constant shear strain, $e_{xy}=(1/2)[\partial u_y/\partial x+\partial u_x/\partial y]$. However, it must be understood that constant strain image values correlate with constant E only under certain idealized, low-contrast conditions.

C. Cyclic, quasistatic imaging

If a shear step is repeated sinusoidally at a relatively slow rate ~e.g., at less than five cycles per second!, then for most practical cases of tissues and organs, the inertial terms of the governing equations can still be neglected. The behavior can be described in the same functional form as the static case, but modified by the addition of a sinusoidal time-varying term. Thus, if the shear plate of Fig. 2 is moved as $u_y(x=0)=U_0\cos\nu_L t$, where ν_L is low frequency, then $u_y(x)=U_0(1-x/d)\cos\nu_L t$ for $0<x<d$, and the resulting strain is similarly time varying. This is shown schematically in Fig. 3. The practical advantages of cyclic quasistatic methods over single-step methods are primarily due to the ability to average and automate, thereby reducing noise and artifacts.[16,35]

D. Shear wave vibration

As the left vertical plate of Fig. 3 is displaced at higher frequencies, the time-varying inertial terms of the governing equation cannot be ignored and the behavior of the medium obeys the classic wave equation.

For a plane wave propagating in the x direction with particle motion in the y direction @$u_y = u_y(x,t)$ and $u_x = u_z = 0$], the shear wave equation @Eq. ~7!#, reduces to a one-dimensional equation of the form

$$\frac{\partial^2 u_y}{\partial x^2} = \frac{1}{c_s^2}\frac{\partial^2 u_y}{\partial t^2}. \qquad \text{~12!}$$

For regular geometries and simple conditions, with low loss or attenuation, the response of the medium will peak at specific eigenfrequencies, with standing wave or eigenmodal patterns produced within the interior. Specifically, these occur when the frequency is such that odd multiples of quarter-wavelengths in the x direction are created. These frequencies are given by

$$f = \quad 2n-1=$$

patterns that can be more easily identified when using multifrequency excitations.

These vibration patterns can be imaged in real time using modified color Doppler techniques and are generally referred to as vibration sonoelastography, or simply, sonoelastography. Specifically, the Doppler spectral variance has been shown to be proportional to the vibration displacement amplitude in a sinusoidal steady state.[38] This can be displayed as a color scale overlay on the B-scan image. It has been shown by theory, by finite element modeling, and by experiments that hard inclusions presen.8(hard)-o7g/ardsirdcby

noelastic vibration image will be comprised of the addition of a homogeneous solution to Eq. ~13! ~right-hand side equal to zero! plus the scattered wave. This is depicted in Fig. 5.

Conceptually, this means that even a very small point inhomogeneity, even one well below the resolution of the imaging system, can be detected as a localized disturbance in the form of a free space Green's function, that is a $1/r$ falloff, as depicted in Fig. 5. This is similar to a small point source of light detected ~and then blurred! by an optical imaging system, even though the point source aperture may be below the nominal resolution of the imaging lens. However, the strength of the inhomogeneity's signature increases with increasing frequency. Simulations and experiments have demonstrated that the sonoelastic image contrast of lesions increases with increasing frequency[8] until other frequency-dependent effects, such as lossy behavior, present a practical upper frequency limitation.[40]

This wave behavior limits the resolvability of two small neighboring points since the Green's function scattered waves pattern produced by each has an inherent type of blur, which will add coherently when the two points are closely spaced. Thus, no general claim for subresolution resolvability can be made, even though a general claim for subresolution detectability can be made.

IV. DISCUSSION AND CONCLUSION

A plethora of techniques for estimating and imaging the elastic properties of tissue have been proposed, each one employing a unique excitation function to create displacements in tissue. We demonstrate, however, that the most commonly utilized methods, from step-compression elastography through vibration ~sono! elastography, fall on a continuum of elastic behavior. The information that can be derived from an ideal imaging system can be used, in each case, to identify an inclusion that is defined by some elastic contrast compared to the background. However, the particular details of preprocessing, detectability, and resolvability do change from static and quasistatic to dynamic systems where wave behaviors are exhibited. Figure 6 compares the shear behavior of a simple homogeneous system as it is excited by different displacement functions along the continuum of frequencies.

As a practical matter, the imaging system ~typically ultrasound or MRI! resolution and noise characteristics will limit the performance of elasticity imaging and reconstruction schemes, along with the other practical limits from tissue motion and loss mechanisms. Specifically, on the static and low-frequency side of the continuum, tissue motion out-of-plane, noise, and speckle decorrelation artifacts from rotations all limit the displacement and derivative of displacement estimations.[39] At the other end of the continuum, the high losses or attenuation of shear waves above 200–400 Hz creates a practical limitation on whole organ penetration and potential increases in lesion contrast that would otherwise be predicted from Eq. ~12!. Lower bounds on correlation-based displacement estimates[40] and Doppler estimates of vibration amplitudes,[38] and MRE detection of vibration[23] have demonstrated very fine scale ~micron or below! possibilities given an adequate signal-to-noise ratio.

There is another important topic of exact inverse solutions ~of unknown elastic properties from the imaging data! that is beyond the scope of this paper. However, a few general remarks can be made. The exact inversion of static and quasistatic cyclic compression cases requires knowledge of boundary conditions that in most cases lie outside of the imaged region of interest. Solving for the unknown stress field ~including localized stress concentrations! is difficult but necessary to utilize the local stress–strain behavior to solve for elastic parameters. In shear wave propagation, however, local estimates of displacement and wave behavior can be used to generate localized estimates of elastic properties,

chanical properties [illegible]es," J. Rehabil. Res. D[illegible]8 ~1987!.
[3] Y. Yamakoshi, J. [illegible] Sato, "Ultrasonic imaging of [illegible]- tions of soft ti[illegible]ced vibration," IEEE Trans. U[illegible]- electr. Freq. [illegible]5–53 ~1990!.
[4] R. M. Lern[illegible]er, J. Holen, R. Gramiak, and R. C. [illegible]- elasticity [illegible]asticity images derived from ultrasc[illegible]n mecha[illegible]ed targets," *Proceedings of the 16th [illegible]l Acou[illegible] Symposium (Plenum)*, 1988, Vol. 16, p[illegible]
[5] R. M[illegible] deriv[illegible] soun[illegible]
[6] K. J. Parker, S. R. Huang, R. A. Musulin, and R. M. L[illegible]e response to mechanical vibrations for 'sonoelasticity ima[illegible]- sound Med. Biol. **16**, 241–246 ~1990!.
[7] L. Gao, K. J. Parker, R. M. Lerner, and S. F. Levinson, "[illegible]e elastic properties of tissue—A review," Ultrasound Med. [illegible]– 977 ~1996!.
[8] K. J. Parker, D. Fu, S. M. Gracewski, F. Yeung, and S[illegible]n, "Vibration sonoleastography and the detectability of lesion[illegible]d Med. Biol. **24**, 1937–1947 ~1998!.
[illegible] L. Gao, K. J. Parker, S. K. Alam, and R. M. Lerner, "Sonoelasticity imaging: Theory and experimental verification," J. Acoust. Soc. Am. **97**, 3875–3880 ~1995!.
[10] S. F. Levinson, M. Shinaguwa, and T. Sato, "Sonoelastic determination of human skeletal muscle elasticity," J. Biomech. **28**, 1145–1154 ~1995!.
[11] F. Yeung, S. F. Levinson, D. Fu, and K. J. Parker, "Feature-adaptive mo-
prD [(,)-332.7(17.6-64.9(–13261)-64.9(1)37(154)]TJ /F8 1 Tf 5.4711 0 TD 0 TD)Tj /F17 1 Tf 0.3334(1990)Tj /F8 1 Tf 129998 0 TD (!)Tj /F17 1 Tf 0.333 0 TD 1.